Top Catal (2016) 59:564–573
DOI 10.1007/s11244-015-0526-2

ORIGINAL PAPER

Heterogeneous Oxygen-Containing Species Formed via Oxygen or Water Dissociative Adsorption onto a Gallium Phosphide Surface

Xueqiang Zhang[1,2] · **Sylwia Ptasinska**[1,3]

Published online: 29 December 2015

Abstract Interactions of O_2 or H_2O with a GaP(111) surface were investigated over wide ranges of pressure and temperature using near-ambient pressure X-ray photoelectron spectroscopy. We demonstrated the formation of several oxygen-containing species from the dissociative adsorption of gas-phase molecules onto GaP(111). Chemical evolutions were determined at the gas/semiconductor interfaces based on changes in the high-resolution photoelectron spectra, which allowed us to identify the final products formed either directly or through intermediate species. We then used the Ga $2p_{3/2}$ spectra to create maps of the relative abundances of surface oxides and hydroxyl groups present under various experimental conditions. In the case of the O_2/GaP(111) interface, we detected Ga–P bonds, and various oxygen-containing species, i.e., Ga_2O, Ga_2O_3, and $GaPO_m$. In the case of the H_2O/GaP(111) interface, in addition to the detection of Ga–P bonds, species were formed with a different extent of oxidation and hydroxylation, O_n–Ga–$(OH)_{3-n}$, via a Ga_2O-like intermediate species. In both cases, the co-existence of multiple species represented as $(GaPO)_A$ or $(GaPOH)_B$, was displayed under specific conditions.

Keywords Near-ambient pressure XPS · Gallium phosphide · Gas/solid interface · Surface oxidation

✉ Sylwia Ptasinska
sylwia.ptasinska.1@nd.edu

[1] Radiation Laboratory, University of Notre Dame, Notre Dame, IN 46556, USA

[2] Department of Chemistry and Biochemistry, University of Notre Dame, Notre Dame, IN 46556, USA

[3] Department of Physics, University of Notre Dame, Notre Dame, IN 46556, USA

1 Introduction

As the world's energy consumption increases, the ability to generate clean and sustainable energy has become imperative. One of the possible methods for producing clean energy is the use of solar power to harvest hydrogen fuel in photoelectrochemical (PEC) cells. Typically, in this method, water in the cell is oxidized into O_2 by holes generated at a photoanode and is reduced into H_2 at a cathode, thereby creating the fuel [1]. The highest solar-to-hydrogen efficiency of 12.4 % was achieved using a $GaInP_2$/GaAs tandem cell [2]. Current material sciences research enhances the efficiency of photocatalytic water-splitting by using III–V semiconductor-based anodes with higher stabilities in aqueous media [3], and with suitable band-edge and band-gap energies, in order to match both the potential for water oxidation–reduction reactions and the solar spectrum, respectively. GaP is a semiconductor that fulfills these criteria. However, it has not yet reached its full potential because the interfacial reactions that occur on its surface under various external/internal conditions, such as high temperature, high current, the influence of electrolytes (e.g., H_2O) and its products, or dissolved environmental contaminants (e.g., O_2), often lead to material corrosion, which shortens the lifetime of PEC cells [4]. The fundamental effects of these factors are still not well understood. Gaining such knowledge is essential to deepen our understanding of the water-splitting mechanisms and to improve the stability of PEC devices in general.

The overall goal of our experimental efforts is to elucidate the mechanisms involved in complex electrolyte/electrode interfacial reactions in PEC cells. We use model systems to investigate the interactions of water, or its electrolysis products with semiconducting surfaces

under near-ambient pressure conditions, which are more relevant to the operational conditions of PEC cells than are ultra-high vacuum (UHV) conditions. It has been reported that the compositional, structural, and electronic properties of a material surface under ambient conditions can differ substantially from those under UHV conditions, because of changes in surface free energies that can vary by 0.3 eV or more [5]. Our recent in situ study of H_2O dissociative adsorption onto the GaP(111) surface under elevated pressures and temperatures showed dynamic chemistry at the H_2O/GaP interface, which resulted in a high degree of surface hydroxylation and oxidation [6]. The results of that study are extended in this work, in which we compare the evolutions of oxygen-containing species formed at the H_2O/GaP(111) and O_2/GaP(111) interfaces, and construct maps that display both the structural transformation and the presence of these species under several experimental conditions. In this study, we used a near-ambient pressure X-ray photoelectron spectroscopy (NAP-XPS) technique to explore the surface interactions between O_2 or H_2O and GaP(111). Using synchrotron radiation, this advanced XPS technique has also been applied successfully by other research groups to study oxidation reactions on Pt-based [7–10], Ir-based [11], ceria [12, 13], perovskite-type [14], and samarium-doped ceria [15] electrodes in a water vapor environment. These investigations with the above-mentioned material electrodes have provided key findings necessary for a fundamental understanding of water-splitting in electrochemical devices and the discovery of innovative solutions for novel types of electrodes. However, scant attention has been paid to H_2O interactions with Ga-based materials, which are one of the most common materials used today for water-splitting, as they help improve electrode stability and thereby enhance PEC performance. A molecular understanding of the surface chemistry on Ga-based materials under ambient conditions is highly desirable in order to enhance the design of future PEC devices. In this work, we used a lab-based NAP-XPS technique to determine the chemical nature of key interfacial reactions between gas and solid semiconductor systems as a first step in the optimization of electrochemical cells.

2 Experimental Set-up

The experimental technique and procedures employed in this study are similar to those reported in our previous work [6, 16–18]. Therefore, we describe them here only briefly. We recorded high-resolution photoelectron spectra using a lab-based NAP-XPS apparatus (SPECS Surface Nano Analysis GmbH, Berlin, Germany). We generated an X-ray beam with a photon energy of 1486.7 eV from an aluminum anode in a micro-focus X-ray (XR-MF) source. The XR-MF source was also equipped with a quartz crystal mirror, which was used for light monochromatization, providing an intrinsic energy resolution of a full width at half maximum (FWHM) of 167 meV for Al Kα. The anode voltage and emission current were set at 15 kV and 6.7 mA, respectively, to produce an X-ray beam with a maximum power of 100 W. Interactions of O_2 or H_2O with GaP(111) took place in a reaction cell, which sustained pressures up to 20 mbar while also heating the crystal to 900 K by electron bombardment on the backside of the sample holder. The GaP(111) crystal was clamped to a molybdenum sample holder with a chromel–alumel thermocouple (K-type) inserted beneath the crystal. A membrane (Si_3N_4) window allowed the X-ray beam to pass through to the reaction cell, where the beam was incident at 54.7° to the crystal surface normal. The crystal was placed in front of a nozzle with an orifice of ~300 μm. Photoelectrons ejected from the crystal passed through the nozzle to the differential pumping electrostatic lens system of a PHOIBOS 150 Hemispherical Energy Analyzer (HEA) and were detected by a nine-single channel electron multiplier (MCD-9). This study was performed over a wide range of pressure (10^{-10} – 5 mbar) and temperature (298–773 K). The O_2 gas (Airgas, USA) had a purity of 99.993 %, and the deionized water (Milli-Q, Millipore) was freeze-pump-thawed several times to remove gaseous contaminants prior to introducing vapor into the reaction cell. The compositions of O_2 and H_2O that flowed through the reaction cell were monitored by a residual gas analyzer (RGA) connected to the differential pumping stage. No significant contaminants (specifically, any that were more than 2–3 orders of magnitude lower than the introduced gas) were measured by the RGA. An undoped planar GaP crystal with a (111) orientation and a resistivity of ~0.3 Ωcm was purchased from Sigma-Aldrich, USA. The GaP (111) crystal was sputtered by a 0.4 keV Ar^+ beam, followed by annealing to ~800 K [19]. The surface cleanliness was examined by taking photoelectron spectra, and the cleaning procedure was repeated until no C 1s nor O 1s signals were detected.

High-resolution spectra were recorded with a pass energy of 20 eV, and an FWHM of 0.5 eV was measured for the Au $4f_{7/2}$ peak. Within 1–1.5 h, we recorded one set of spectra taken at a binding energy (BE) region for each particular element. Typically, minor changes (<5 %) in the spectra were observed for a prolonged time (>2 h) at elevated pressures and temperatures below 673 K. However, above temperatures of 673 K, faster and more pronounced changes (~15 %) were observed. Therefore, spectra were taken within a shorter acquisition time to follow the time-dependent chemical evolution or to verify possible evaporation of volatile compounds. We used the P $2p_{3/2}$ peak at

128.8 eV, corresponding to P–Ga for the BE scale calibration [6]. Analyses of all spectra were performed using CasaXPS software by fitting Gaussian/Lorentzian (G/L) hybrid functions fixed at defined BE values (±0.1–0.2 eV), FWHMs (±0.4 eV), and G/L mixing ratios. The G/L mixing ratio was 70:30 for Ga $2p_{3/2}$ and 30:70 for P 2p. The chemical shifts in BEs with respect to the BE of peaks for clean GaP were consistent with those reported previously [6, 16–18, 20–28]. Along with the O 1s and P 2p spectra, we chose the Ga $2p_{3/2}$ spectra for the interfacial chemistry analysis because of their greater surface-sensitive characteristics in comparison with Ga 3d spectra. Tables 1 and 2 list the BE values used for the peak fitting, which correspond to various possible surface species formed from O_2 and H_2O interactions, respectively.

3 Results and Discussion

In order to track the formation of oxygen- and hydroxyl-containing species on the surface of GaP(111) at near-ambient conditions, we recorded high-resolution spectra of Ga $2p_{3/2}$, P 2p, and O 1s over wide ranges of O_2 or H_2O pressure and crystal temperature. Figure 1 shows the evolution of Ga $2p_{3/2}$ spectra under various experimental conditions, including a pressure-dependent study, in which GaP(111) was kept at room temperature (298 K) while either O_2 or H_2O was introduced at several pressures, and a temperature-dependent study, in which the pressure of either O_2 or H_2O was kept constant (0.1 mbar) while the temperature of GaP(111) varied.

The pressure-dependent studies showed minor but visible changes, which were detected in the Ga $2p_{3/2}$ spectra. For a clean GaP(111) surface under UHV conditions, the maximum of the Ga $2p_{3/2}$ peak was located at a BE of 1117.3 eV, corresponding to pure Ga–P bonds [6]. The appearance of a low-intensity signal at a higher BE was observed at O_2 or H_2O pressures as low as 5×10^{-3} mbar, and was enhanced gradually by an increase in gas pressure. In the case of O_2 interactions with GaP(111) at elevated pressures, the appearance of a higher BE shoulder indicated an initial oxidation process involving the chemisorption and dissociation of O_2, along with a subsequent incorporation of an O atom into the surface of GaP(111) [29]. In the case of H_2O interactions with GaP(111) at elevated pressures, the spectra showed more pronounced changes in the peak shape of Ga $2p_{3/2}$ in comparison with the corresponding spectra for elevated pressures of O_2, indicating the formation of different surface species from the H_2O dissociative adsorption. As presented later in this work, this higher BE shoulder was attributed primarily to surface hydroxyl- and oxygen-containing species formed at the H_2O/GaP(111) interface. The formation of oxygen-containing species in both pressure-dependent experiments was also evident by the appearance of the O 1s signal. However, only minor changes were observed in the P 2p spectra as the O_2 or H_2O pressure increased. Nevertheless, P sites on the GaP surface have an anionic character, and therefore can form thermodynamically stable P–H bonds in the case of the H_2O/GaP(111) interface and can play an essential role in H_2O dissociation, as predicted by previous calculations [30–32]. Correspondingly, our study of the H_2O/GaAs(100) interface indicated the possible formation of As–H bonds at near-ambient conditions, as shown by chemical shifts in the As 2p spectra [16, 33]. In the case of the O_2 interactions, the greater extent of oxidation of Ga

Table 1 Values of binding energy used in peak fitting of Ga $2p_{3/2}$, O 1s, and P 2p spectra for the O_2/GaP(111) interface

Elemental spectrum	BE (eV)	Species	Peak labeling	References
Ga $2p_{3/2}$	1117.3	Ga–P	4	6, 20
	1117.7	Ga_2O	3	17, 21, 22, 24-26
	1118.3	Ga_2O_3	2	17, 21, 22, 24-26
	1118.8	$GaPO_m$	1	6, 26
P 2p	128.8	P–Ga ($2p_{3/2}$)	9	6, 20
	129.6	P–Ga ($2p_{1/2}$) and P–P or P–Ga (P $2p_{3/2}$) affected by adsorbates (O_2, O)	8	6, 28, 40, 41
	130.4	P–P or P–Ga (P $2p_{1/2}$) affected by adsorbates (O_2, O)	7	6, 28, 40, 41
	134.3	$GaPO_4$ $GaPO_m$	6	6, 26
	135.2	$Ga(PO_3)_3$	5	6, 26
O 1s	530.6	Ga–O–Ga	12	6, 16-18
	531.8	$GaPO_4$ and $Ga(PO_3)_3$	11	6
	532.2	Chemisorbed O	10	6, 17

Peak labeling corresponds to that in Fig. 2

Table 2 Values of binding energy used in peak fitting of Ga $2p_{3/2}$, O 1s, and P 2p spectra for the H_2O/GaP(111) interfaces

Elemental spectrum	BE (eV)	Species	Peak labeling	References
Ga $2p_{3/2}$	1117.3	Ga–P	4	6, 20
	1117.7	Ga_2O-like	3	6, 24–26
	1118.0	HO–Ga–O	2	6, 16, 23
	1119.2	O_n–Ga–$(OH)_{3-n}$	1	6, 16
P 2p	128.8	P–Ga ($2p_{3/2}$)	9	6, 20
	129.6	P–Ga ($2p_{1/2}$)/P–H ($2p_{3/2}$)	8	6, 16, 31
	130.4	P–H ($2p_{1/2}$)	7	6, 16, 31
	134.2	P oxides and hydroxides	6	6, 26
	135.1		5	6, 26
O 1s	530.6	Ga–O–Ga	15	6, 16–18
	531.3	OH	14	6, 14–16
	531.7	HO–H_2O	13	6, 14–16
	532.1	O_n–Ga–$(OH)_{3-n}$	12	6, 16
	532.6	Molecularly adsorbed H_2O	11	6, 14–16
	533.1	P oxides	10	6, 26

Peak labeling corresponds to that in Fig. 3

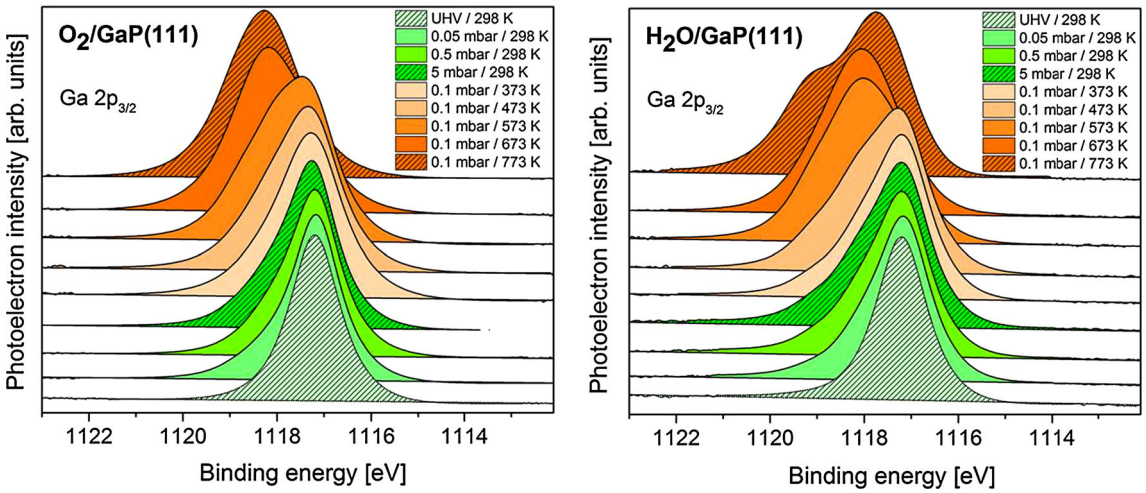

Fig. 1 Evolutions of Ga $2p_{3/2}$ spectra obtained at the O_2/GaP(111) and H_2O/GaP(111) interfaces under various experimental conditions. These spectra were normalized to the same unit of intensity

atoms than their counter element in the GaAs crystals has been explained previously by the fact that the formation of Ga oxides is thermodynamically more favorable than that of As oxides [17, 18, 25]. This pressure-dependent study showed only a low extent of surface oxidation; nevertheless, it is important to note that the activity of the GaP surface was high enough to induce O_2 or H_2O chemisorption, dissociation, and Ga–O bond formation at 298 K. In addition to fragmentation processes, our previous studies on the H_2O/GaP(111) interface showed the simultaneous existence of undissociated H_2O molecules on the surface [6]. Surface H_2O molecules could be adsorbed directly by two lone-electron pairs onto an empty hybrid p-orbital of Ga [30, 31, 34, 35], or attached indirectly to GaP(111) by surface-anchoring OH groups [20, 36, 37], or bonded to neighboring H_2O molecules to form hydrogen-bond networks [7, 10]. These three forms contributed to changes in the O 1s spectra at elevated pressures, and they remained even after the H_2O molecules were pumped away from the reaction cell. Furthermore, the reason for the preferential oxidation of Ga over P for O_2 interactions with GaP(111) is still not well understood. One of the possible factors could be the lower electronegativity of Ga and thus its higher affinity for O_2 attachment. As reported for the O_2/InP interface, O_2 dissociates directly and forms chemical bonds with the III-group element, thereby causing its

oxidation [38]. In contrast, for the O_2/GaAs interface, O_2 adsorbs dissociatively at first onto the V-group element and then the O product is transferred to the III-group element, thereby leading to Ga oxidation [39].

Based on the Ga $2p_{3/2}$ spectra in Fig. 1, we observed a much more dynamic chemistry in the temperature-dependent study. In the case of the H_2O/GaP(111) interface, two distinct regions were defined, one below and one above 673 K. Below 673 K, the signal that appeared at the high BE side was extended by an increase in temperature and caused a chemical shift of the maximum intensity toward higher BEs in the Ga $2p_{3/2}$ spectra. Above 673 K, a large-scale conversion of the surface species occurred, which was observed as a splitting of the peak maximum into two components at BEs of ~1117.5 and 1119 eV. In the case of the O_2/GaP(111) interface, below 573 K, there was a smooth shift of the peak maximum toward higher BEs, caused primarily by a broadening of the Ga $2p_{3/2}$ peak. When the temperature exceeded 573 K, a sudden 0.5 eV shift of the peak in the Ga $2p_{3/2}$ spectrum occurred, indicating the splitting of Ga–P bonds and enhanced oxidation of the GaP(111) surface.

In general, at near-ambient conditions, the GaP(111) surface consisted of heterogeneous species, which can be represented by the formulas $(GaPO)_A$ and $(GaPOH)_B$, where "A" and "B" represent the various possible stoichiometries of these elements, in the case of the O_2/GaP(111) and H_2O/GaP(111) interfaces, respectively. To identify the types of species formed on the GaP(111) surface under these different conditions, Figs. 2 and 3 present the fitted high-resolution Ga $2p_{3/2}$, P 2p, and O 1s spectra for the O_2/GaP(111) and H_2O/GaP(111) interfaces, respectively. These two figures contain peak assignments for possible chemical structures formed on GaP(111), whose BE values were determined based on earlier extensive XPS studies of III-V semiconductors under UHV conditions (InP [28] and GaP [27]) and at near-atmospheric pressure conditions (GaP [6] and GaAs [16–18, 33]), which are listed in Tables 1 and 2. It is worth noting that these oxides and hydroxyls did not necessarily indicate stoichiometric and pure compounds because they were formed under non-equilibrium thermodynamic conditions. Thus, the surface was likely composed of heterogeneous oxygen- and hydroxyl-containing species, forming an amorphous surface layer.

The UHV Ga $2p_{3/2}$ spectrum exhibited one peak that was attributed to the pure Ga–P bond. The corresponding P 2p spectrum exhibited two closely spaced spin–orbit components, i.e., $2p_{1/2}$ and $2p_{3/2}$, with a ratio of 1:2 (Fig. 2). As shown in Fig. 2, both the elemental signals decreased due to a scattering of photoelectrons with gas-phase molecules at an O_2 pressure of 5 mbar. This decrease

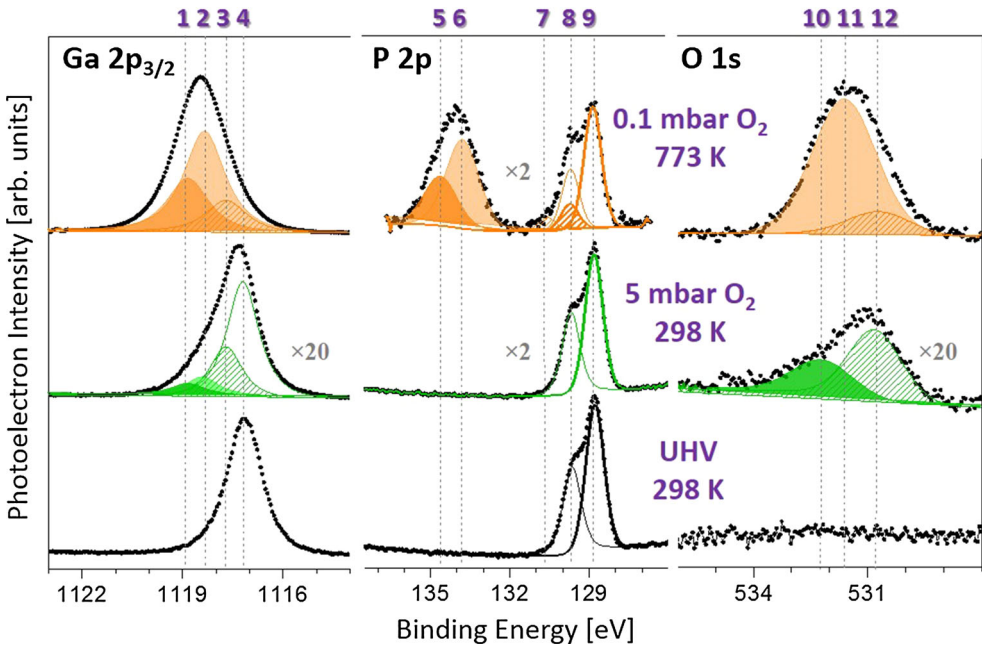

Fig. 2 Fitted spectra obtained at three different pressure/temperature conditions for Ga $2p_{3/2}$, P 2p, and O 1s at the O_2/GaP(111) interface. Due to photoelectron scattering with O_2 at elevated pressures or P depletion at high temperatures, the spectral intensities were enlarged by the factors indicated. Each fitted *line* corresponds to the possible oxygen-containing species listed as follows: *1* $GaPO_m$, *2* Ga_2O_3, *3* Ga_2O, *4* Ga–P, *5* $Ga(PO_3)_3$, *6* $GaPO_4$, *7* P–P or P–Ga (P $2p_{1/2}$) affected by adsorbates (O_2, O), *8* P–Ga ($2p_{1/2}$) (*higher peak*) and P–P or P–Ga (P $2p_{3/2}$) affected by adsorbates (O_2, O) (*lower peak*), *9* P–Ga ($2p_{3/2}$), *10* chemisorbed O; *11* $GaPO_4$ and $Ga(PO_3)_3$, and *12* Ga–O–Ga

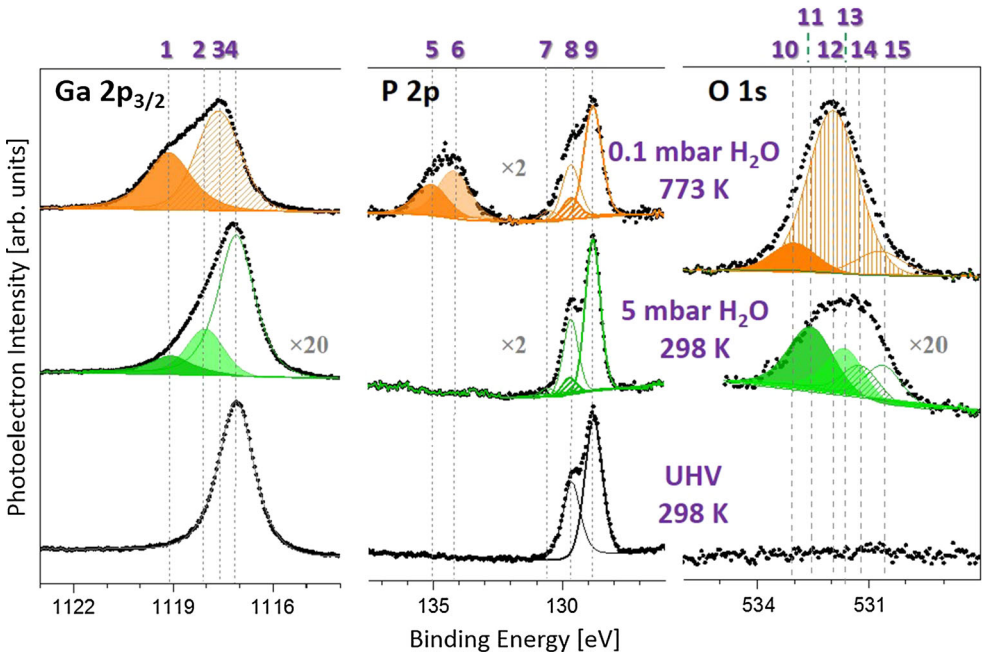

Fig. 3 Fitted spectra obtained at three different pressure/temperature conditions for Ga $2p_{3/2}$, P 2p, and O 1s at the H_2O/GaP(111) interface. Due to photoelectron scattering with H_2O at elevated pressures, the spectral intensities were enlarged by the factors indicated. Each fitted line corresponds to the possible oxygen- and hydroxyl-containing species listed as follows: *1* O_n–Ga–$(OH)_{3-n}$ ($0 \leq n \leq 1$), *2* O–Ga–OH, *3* Ga_2O-like species, *4* Ga–P, *5* and *6* P oxides and hydroxides, *7* P–H ($2p_{1/2}$), *8* P–Ga ($2p_{1/2}$) (*higher peak*) and P–H ($2p_{3/2}$) (*lower peak*), *9* P–Ga ($2p_{3/2}$), *10* P oxides, *11* molecularly adsorbed H_2O, *12* O_n–Ga–$(OH)_{3-n}$, *13* OH—H_2O, *14* OH, *15* Ga–O–Ga

was more significant for Ga $2p_{3/2}$ than for P 2p, due to the lower kinetic energy of the Ga 2p photoelectrons. Moreover, we observed an asymmetric peak in the Ga $2p_{3/2}$ spectrum, with a signal extension toward higher BEs due to the dissociative adsorption of O_2 and subsequent oxidation of GaP(111). Under these conditions, apart from the presence of pure Ga–P bonds, species with Ga–O bonds also formed on the surface. These species were attributed to the suboxide (Ga_2O) with a bridge structure of Ga–O–Ga. As reported by other research groups, surface Ga–O–Ga or Ga–O–P bridges can trap charge carriers and contribute to photocorrosion [30, 31]. It is important to note that the shape of the Ga $2p_{3/2}$ peak recorded under such conditions remained the same after pumping the O_2 gas out of the reaction cell. This confirmed the formation of long-lasting and chemically-bonded surface species, indicating irreversible surface changes. The Ga $2p_{3/2}$ spectrum at 773 K differed drastically from that obtained at 298 K. A much broader feature was observed with a peak maximum shifted more than 1 eV toward a higher BE. This peak contained contributions from various oxide species, i.e., Ga_2O, Ga_2O_3, and $GaPO_m$, where "m" indicates the unknown-composition stoichiometry of this surface compound, as shown in Fig. 2. The formation of various oxides at these extreme conditions was also supported by the O 1s spectra. The FWHM of the O 1s peak was ~3 eV with a maximum at a BE of 532.5 eV, implying the formation of $GaPO_m$ [6, 38, 40]. In contrast, the peak maximum was located at a BE of 530.6 eV, and had a signal intensity reduced significantly at an O_2 pressure of 0.1 mbar and 298 K. This signal was attributed mainly to the Ga–O–Ga structure [6], while we attributed the higher BE shoulder at ~532 eV to chemisorbed O [17, 22]. We observed no significant changes in the P 2p spectra representing the P–Ga bonds at 298 K for different pressures, e.g., UHV and at an O_2 pressure of 5 mbar. However, at a pressure of 0.1 mbar and a temperature of 773 K, a signal appeared at ~134 eV that corresponded to the formation of $GaPO_m$. This new multipeak feature, which appeared at a BE of 134 eV in the P 2p spectra and originated from the $GaPO_m$ species, could correspond to $GaPO_4$ and $Ga(PO_3)_3$ [38, 40–43]. The $GaPO_4$ species were likely to have been produced, because they have also been reported to be primary reaction products of O_2 interactions with GaP [44, 45]. Our recent study of the O_2/GaP(111) interface showed that a further increase in temperature resulted in a total quenching of the P 2p signal.[1] Such changes indicate that a large-scale oxidation of GaP(111) occurred with an estimated oxide layer thickness of ~40 Å, while under 298 K, the oxide thickness was estimated to be only a few Å.

An analogous peak analysis was conducted for spectra obtained from the H_2O/GaP(111) interface (Fig. 3).

[1] unpublished data.

However, due to the greater number of species formed, the peak assignments were more complex. The Ga $2p_{3/2}$ spectra obtained at an H_2O pressure of 5 mbar and 298 K consisted of three components that corresponded to Ga–P bonds, and species containing a different number of hydroxyl groups, O–Ga–OH and O_n–Ga–$(OH)_{3-n}$ ($0 \leq n \leq 1$) on the surface. The latter two structures, i.e., O–Ga–OH and O_n–Ga–$(OH)_{3-n}$, represent non-stoichiometric hydroxide and/or oxide-related compounds, and the BE of O_n–Ga–$(OH)_{3-n}$ was similar to the BE of stoichiometric Ga hydroxides (Ga–$(OH)_3$) [6, 23]. The O 1s spectra consisted of several different species. For example, the spectrum recorded at an H_2O pressure of 5 mbar and at 298 K clearly exhibited two maxima: a lower BE maximum at ~532 eV, consisting of Ga–O–Ga and Ga–OH components, and higher BE components representing undissociated H_2O molecules adsorbed onto the surface [6, 10, 16, 46]. The possible forms of H_2O adsorption were mentioned above. In the case of the O 1s spectra, we used peaks with a relatively larger FWHM in order to limit the numbers of fitted peaks to these broad, poorly resolved spectra. Spectral feature assignments, i.e., the number of fitted peaks corresponding to particular species or structures and their BEs, were based on and were also consistent with previous in situ XPS work on H_2O adsorption and dissociation onto metallic surfaces [5, 46, 47] and Ga-based materials [16, 33]. Therefore, after careful consideration of the possible products formed upon the dissociative adsorption of molecules on the GaP surface, we assigned our peaks accordingly as shown in Table 2.

The peak area ratio of the dissociated products and undissociated H_2O molecules was approximately 6:1 after H_2O was pumped away from the reaction cell [6]. This ratio suggests a high fragmentation yield of H_2O molecules resulting in the oxidation and hydroxylation of the GaP(111) surface [6]. In addition to these changes in the Ga $2p_{3/2}$ and O 1s spectra, only relatively minor changes were observed in the P 2p spectra at elevated H_2O pressures. As has been shown by computational modeling, upon dissociation onto GaP surfaces, the H_2O molecule produces OH and H fragments that interact with Ga and P atoms to form Ga–OH and P–H bonds, respectively [30–32, 34, 35]. Based on peak broadening and shifts in the As $2p_{3/2}$ spectra, our previous study of H_2O interactions with the GaAs(100) surface suggest the formation of an As–H bond at elevated pressures [16, 33]. In this study, the changes observed in the P 2p spectra were less pronounced than were those for GaAs(100). However, this smaller effect of H_2O on GaP(111) does not exclude the possibility of P–H bond formation, but could instead be due to the greater contribution of P 2p photoelectrons from deeper underlying layers in the spectra, as these photoelectrons possess a longer inelastic mean free path than do As 2p photoelectrons [48].

As we concluded from the O_2/GaP(111) study, higher temperatures enhance interactions and the dissociation of gas molecules on the GaP(111) surface, which is also the case at the H_2O/GaP(111) interface. In Fig. 3, all three elemental spectra obtained at an H_2O pressure of 0.1 mbar and a temperature of 773 K exhibited evident changes and the formation of species with structures containing oxidized and/or hydroxylated Ga–P bonds, i.e., $(GaPOH)_B$. The Ga $2p_{3/2}$ spectrum developed a strong signal that we attribute to O_n–Ga–$(OH)_{3-n}$, and together with the appearance of a peak at a BE of 1117.7 eV, hereafter is denoted as a Ga_2O-like species [6]. Simultaneously, Ga–P and O–Ga–OH peaks were quenched completely. The same behavior was also observed in Ga 3d spectra, indicating a chemical restructuring of the deeper layers. It is important to note that Ga_2O-like species were unstable and their signal decreased gradually, while the O_n–Ga–$(OH)_{3-n}$ signal increased [6]. The formation of $(GaPOH)_B$ was also confirmed by P 2p spectra that exhibited a new peak structure at a BE higher than 133 eV (Fig. 3). In the case of the O 1s spectra at elevated pressures, higher BE peaks, corresponding to undissociative H_2O molecules, vanished along with the formation of other oxygen-containing species attributed to the $Ga(OH)_3$ structure and to P oxides. The Ga:P:O ratio changed from 55:45:0 under UHV conditions to 32:24:44 and 30:27:43 at 773 K for 0.1 mbar O_2 and 0.1 mbar H_2O, respectively.

Figure 4a displays the co-existence of several chemical structures as a function of GaP(111) temperature and O_2 or H_2O pressures. In the case of the O_2/GaP(111) interface, four species were present, i.e., Ga–P, Ga_2O, Ga_2O_3, and $GaPO_m$. The relative abundances were obtained from high-resolution Ga $2p_{3/2}$ spectra that were fitted according to Fig. 2. At low O_2 pressures, pure Ga–P bonds were relatively stable over a wide range of temperatures, even up to 773 K; however, at 298 K, the influence of O_2 at 1 mbar caused the evident formation of Ga_2O with a relative percentage above 25 %. As shown in Fig. 4a, Ga_2O species can also be formed at much lower O_2 pressures, i.e., as low as 5×10^{-3} mbar, if the temperature of GaP(111) is sufficiently high, ~500 K. These Ga_2O species were composed of Ga–O–Ga bridges, which are more stable by 0.5 eV than are Ga–O–P bridges [34]. However, under extreme conditions, Ga_2O was absent, indicating that these were intermediate species that converted to other oxide products. The border of the region, where the presence of pure Ga–P bonds diminished, overlapped with that in which the formation of Ga_2O_3 was initiated, confirming that a large number of Ga–P bonds must be broken in order to incorporate O atoms and produce Ga_2O_3. Under the extreme conditions of our experiments, two final products were observed, i.e., Ga_2O_3 and $GaPO_m$. However, it was difficult to estimate the relative ratio of these two phases

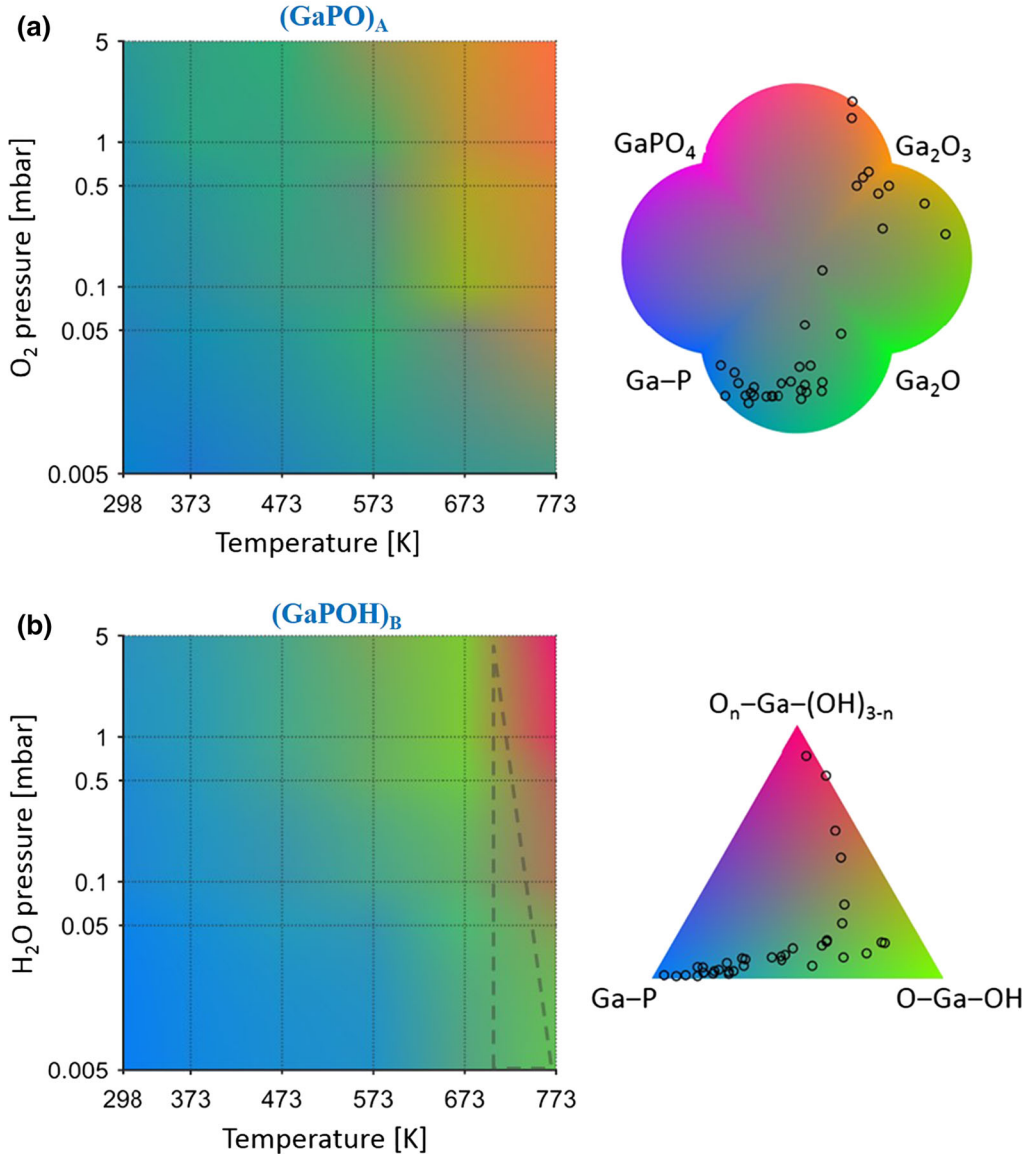

Fig. 4 *Left* maps representing overlays of multiple oxygen-containing species with their relative abundances as a function of **a** O_2 and **b** H_2O pressures, and GaP(111) temperatures obtained from GaP $2p_{3/2}$ spectra. Crossing of grids represents points where the spectra were measured; the values between measured points are bi-linearly interpolated. The *dashed outline* in (**b**) shows the conditions under which the intermediate Ga_2O-like species were formed at the H_2O/GaP(111) interface. The presence of Ga_2O-like species was time-dependent, and therefore, they were not included in the color legend. *Right* the *color legends* indicate the mixing of these species. Each concave point or vertice represents the relative abundance of 100 % of a particular species. The contributions of the species decreased linearly to zero along adjacent edges and was zero along the opposite edges. The center of the legend represents an equal contribution from all species, i.e., 25 % for the O_2/GaP(111) interface and 33 % for the H_2O/GaP(111) interface. *Black circles* correspond to the crossing of grids on the maps

because under these conditions, a prolonged acquisition time induced further chemical changes. Moreover, some surface Ga–P bonds were still preserved along with the Ga_2O_3 products. When the $GaPO_m$ species are predominantly present, however, no more pure Ga–P bonds were detected. The absence of Ga–P bonds indicated that, in order to form $GaPO_m$ species, structural changes occurred on a large scale, and were accompanied by the incorporation of O into such bonds. The oxidation processes that occurred under higher temperature conditions, and which were far from thermodynamic equilibrium, produced long-lasting products. These products were also detected after the crystal was cooled and the O_2 molecules were pumped away.

Figure 4b shows an overlay of the regions where various species were detected at the H_2O/GaP(111) interface. No previous work has provided maps of the relative abundances of these species. As seen from this map, the presence of Ga–P bonds was observed over relatively large

ranges of H_2O pressure and crystal temperature. The O–Ga–OH species formed due to H_2O dissociation were observed predominantly above 600 K, even at H_2O pressures as low as 5×10^{-3} mbar. Their formation increased strongly with an increase in H_2O pressure, indicating enhanced H_2O dissociation. This was also accompanied by a higher extent of OH-related species on the surface, assigned as O_n–Ga–$(OH)_{3-n}$ species in Fig. 4b. It is important to note that prolonged surface exposure to H_2O above a temperature of 773 K induced clear time-dependent changes in the GaP surface chemistry [6] under specific conditions, marked as a dashed outline in Fig. 4b. The species that formed temporarily were assigned as Ga_2O-like species, since their BE value in the Ga $2p_{3/2}$ spectra, shown in Fig. 3, matched the BE value for stoichiometric Ga_2O [25, 26]. The time-dependent study showed a gradual signal quenching of these intermediate species along with an increase in the signal for O_n–Ga–$(OH)_{3-n}$ species [6]. Finally, at elevated pressures and temperatures, the surface evolved into a chemical state that corresponds largely to Ga terminated by hydroxyl groups. Moreover, because the final products, Ga hydroxides, were formed along with P oxides, as shown in Fig. 3, we propose that the multiple species $(GaPOH)_B$ were most likely to have the O = P(Ga–OH)–O(H)–Ga structure [6]. The presence of Ga–O–P bridges at the H_2O/GaP(111) interface contrasted with the structures observed at the O_2/GaP(111) interface, i.e., Ga–O–Ga, which, based on computational modeling, are more stable [34]. Thus, at high temperatures, P oxidation initiated by H_2O dissociation was predominantly a kinetically-controlled process. Similar to the case of O_2 interactions, the oxidation and hydroxylation processes that occurred under higher temperature conditions, which were far from thermodynamic equilibrium, produced long-lasting products that were also detected after the crystal was cooled and the H_2O molecules were pumped away.

4 Conclusions

Using the NAP-XPS technique, the physicochemical processes on the surface of GaP(111) were tracked in situ over a wide range of O_2 and H_2O pressures and crystal temperatures. This technique allowed us to detect intermediate species, which catalyzed the dissociation of gas molecules and led to the final oxygen-containing products. These oxides and hydroxyls do not necessarily indicate stoichiometric and pure compounds, as they formed under conditions that were not in thermodynamic equilibrium. Thus, the surface was likely to be composed of amorphous and nonstoichiometric species, or even a mixture of several species. Such heterogeneous species can be represented by the formulas $(GaPO)_A$ and $(GaPOH)_B$, having various elemental stoichiometries, in the case of the O_2/GaP(111) and H_2O/GaP(111) interfaces, respectively. The conditions under which specific species were present have been visualized as maps, which are also useful in tracking chemical reactions, including the formation of intermediates and their transformation to the final products.

As previous studies have reported, the formation of oxygen-containing species in the forms of Ga–O–Ga or Ga–O–P bridges can enhance H_2O dissociation by accepting H from an H_2O molecule. Thus, the oxides and/or hydroxyls produced can be the reactants of further dissociation [31, 32]. However, a highly oxidized GaP surface can initiate a photocorrosion process in GaP-based PEC cells. The above-mentioned bridges can trap carrier holes that affect the corrosion and performance of the PEC device. Therefore, these findings on the chemical transformation of semiconducting surfaces due to their interactions with O_2 and H_2O are essential for gaining a deeper understanding of oxidation mechanisms at the gas/semiconductor interface, and can lead to improvements in the performance and stability of the PEC cell.

Acknowledgments This material is based upon work supported by the U.S. Department of Energy Office of Science, Office of Basic Energy Sciences under Award Number DE-FC02-04ER15533. This is contribution number NDRL 5069 from the Notre Dame Radiation Laboratory. The authors would like to thank James Kapaldo for creating the two maps using the MATLAB software.

References

1. Gratzel M (2001) Nature 414:338–344
2. Young JL, Doescher H, Steiner MA, Palay E, George SM, Deutsch TG, Turner JA (2015) MRS-Spring Meeting, San Francisco
3. Hu S, Shaner MR, Beardslee JA, Lichterman M, Brunschwig BS, Lewis NS (2014) Science 344:1005–1009
4. Kaiser B, Fertig D, Ziegler J, Klett J, Hoch S, Jaegermann W (2012) ChemPhysChem 13:3053–3060
5. Salmeron M, Schlogl R (2008) Surf Sci Rep 63:169–199
6. Zhang X, Ptasinska S (2015) Phys Chem Chem Phys 17:3909–3918
7. Arrigo R, Havecker M, Schuster ME, Ranjan C, Stotz E, Knop-Gericke A, Schlogl R (2013) Angew Chem Int Ed 52:11660–11664
8. Takagi Y, Wang H, Uemura Y, Ikenaga E, Sekizawa O, Uruga T, Ohashi H, Senba Y, Yumoto H, Yamazaki H, Goto S, Tada M, Iwasawa Y, Yokoyama T (2014) Appl Phys Lett 105:131602–131606
9. El Gabaly F, McDaniel AH, Grass M, Chueh WC, Bluhm H, Liu Z, McCarty KF (2012) Chem Commun 48:8338–8340
10. Casalongue HS, Kaya S, Viswanathan V, Miller DJ, Friebel D, Hansen HA, Norskov JK, Nilsson A, Ogasawara H (2013) Nat Commun 4:2817
11. Casalongue HGS, Ng ML, Kaya S, Friebel D, Ogasawara H, Nilsson A (2014) Angew Chem Int Ed 53:7169–7172
12. Zhang CJ, Yu Y, Grass ME, Dejoie C, Ding WC, Gaskell K, Jabeen N, Hong YP, Shayorskiy A, Bluhrn H, Li WX, Jackson

GS, Hussain Z, Liu Z, Eichhorn BW (2013) J Am Chem Soc 135:11572–11579
13. Zhang CJ, Grass ME, Yu Y, Gaskell KJ, DeCaluwe SC, Chang R, Jackson GS, Hussain Z, Bluhm H, Eichhorn BW, Liu Z (2012) ACS Catal 2:2297–2304
14. Opitz AK, Nenning A, Rameshan C, Rameshan R, Blume R, Havecker M, Knop-Gericke A, Rupprechter G, Fleig J, Klotzer B (2015) Angew Chem Int Ed 54:2628–2632
15. Feng ZLA, El Gabaly F, Ye XF, Shen ZX, Chueh WC (2014) Nat Commun 5:4374
16. Zhang X, Ptasinska S (2014) J Phys Chem C 118:4259–4266
17. Zhang X, Ptasinska S (2015) J Phys Chem C 119:262–270
18. Zhang X, Lamere E, Liu X, Furdyna JK, Ptasinska S (2014) Appl Phys Lett 104:181602–181606
19. Xu G, Hu WY, Puga MW, Tong SY, Yeh JL, Wang SR, Lee BW (1985) Phys Rev B 32:8473–8476
20. Iwasaki H, Mizokawa Y, Nishitani R, Nakamura S (1979) Surf Sci 86:811–818
21. Priyantha W, Radhakrishnan G, Droopad R, Passlack M (2011) J Cryst Growth 323:103–106
22. Epp JM, Dillard JG (1990) Chem Mater 2:449–454
23. Epp JM, Dillard JG (1989) Chem Mater 1:325–330
24. McDonnell S, Dong H, Hawkins JM, Brennan B, Milojevic M, Aguirre-Tostado FS, Zhernokletov DM, Hinkle CL, Kim J, Wallace RM (2012) Appl Phys Lett 100:141606–141609
25. Brennan B, Zhernokletov DM, Dong H, Hinkle CL, Kim J, Wallace RM (2012) Appl Phys Lett 100:151603–151606
26. Hinkle CL, Vogel EM, Ye PD, Wallace RM (2011) Curr Opin Solid State Mater Sci 15:188–207
27. May MM, Supplie O, Hohn C, Van De Krol R, Lewerenz HJ, Hannappel T (2013) New J Phys 15:103003
28. May MM, Lewerenz HJ, Hannappel T (2014) J Phys Chem C 118:19032–19041
29. Ketteler G, Ogletree DF, Bluhm H, Liu HJ, Hebenstreit ELD, Salmeron M (2005) J Am Chem Soc 127:18269–18273
30. Wood BC, Ogitsu T, Schwegler E (2012) J Chem Phys 136:064705–064715
31. Wood BC, Schwegler E, Choi WI, Ogitsu T (2013) J Am Chem Soc 135:15774–15783
32. Wood BC, Schwegler E, Choi WI, Ogitsu T (2014) J Phys Chem C 118:1062–1070
33. Zhang X, Lamere E, Liu X, Furdyna JK, Ptasinska S (2014) Chem Phys Lett 605–606:51–55
34. Jeon S, Kim H, Goddard WA, Atwater HA (2012) J Phys Chem C 116:17604
35. Munoz-Garcia AB, Carter EA (2012) J Am Chem Soc 134:13600–13603
36. Khaselev O, Turner JA (1998) J Electrochem Soc 145:3335–3339
37. Mazin BA, Sank D, McHugh S, Lucero EA, Merrill A, Gao JS, Pappas D, Moore D, Zmuidzinas J (2010) Appl Phys Lett 96:102504
38. Chen G, Visbeck SB, Law DC, Hicks RF (2002) J Appl Phys 91:9362–9367
39. Su CY, Lindau I, Chye PW, Skeath PR, Spicer WE (1982) Phys Rev B 25:4045–4068
40. Hollinger G, Bergignat E, Joseph J, Robach Y (1985) J. Vac Sci Technol 3:2082–2088
41. Brennan B, Dong H, Zhernokletov D, Kim J, Wallace RM (2011) Appl Phys Exp 4:125701
42. Tourtin F, Armand P, Ibanez A, Tourillon G, Philippot E (1998) Thin Solid Films 322:85–92
43. Adelmann C, Cuypers D, Tallarida M, Rodriguez LNJ, De Clercq A, Friedrich D, Conard T, Delabie A, Seo JW, Locquet JP, De Gendt S, Schmeisser D, Van Elshocht S, Caymax M (2013) Chem Mater 25:1078–1091
44. Schwartz GP, Gualtieri GJ, Griffiths JE, Thurmond CD, Schwartz B (1980) J Electrochem Soc 127:2488–2499
45. Schwartz GP (1983) Thin Solid Films 103:3–16
46. Andersson K, Ketteler G, Bluhm H, Yamamoto S, Ogasawara H, Pettersson LGM, Salmeron M, Nilsson A (2008) J Am Chem Soc 130:2793–2797
47. Andersson K, Ketteler G, Bluhm H, Yamamoto S, Ogasawara H, Pettersson LGM, Salmeron M, Nilsson A (2007) J Phys Chem C 111:14493–14499
48. Powell CJ, Jablonski A (2010) NIST standard reference database 71: NIST electron inelastic mean free path database: version 1.2. National Institute of Standards and Technology: Gaithersburg, Maryland, USA